ISSN 0021-8944, Journal of Applied Mechanics and Technical Physics, 2017, Vol. 58, No. 5, pp. 826–836. © Pleiades Publishing, Ltd., 2017.
Original Russian Text © D.V. Khotyanovsky, A.N. Kudryavtsev.

DIRECT NUMERICAL SIMULATION OF THE TRANSITION TO TURBULENCE IN A SUPERSONIC BOUNDARY LAYER ON SMOOTH AND ROUGH SURFACES

D. V. Khotyanovsky and A. N. Kudryavtsev

UDC 532.5.032, 533.6.011.5

Abstract: Direct numerical simulations of instability development and transition to turbulence in a supersonic boundary layer on a flat plate are performed. The computations are carried out for moderate supersonic (free-stream Mach number M = 2) and hypersonic (M = 6) velocities. The boundary layer development is simulated, which includes the stages of linear growth of disturbances, their nonlinear interaction, stochastization, and turbulent flow formation. A laminar–turbulent transition initiated by distributed roughness of the plate surface at the Mach number M = 2 is also considered.

Keywords: direct numerical simulation, laminar–turbulent transition, supersonic boundary layer, distributed roughness.

DOI: 10.1134/S002189441705008X

INTRODUCTION

The study of the laminar–turbulent transition is one of the most challenging problems of fluid mechanics. Researchers pay much attention to this problem because the onset of turbulence significantly alters the flow properties. When the laminar–turbulent transition occurs in the boundary layer, the drag force and the heat fluxes on the body surface are substantially enhanced. Therefore, refinement of the mechanisms of turbulence origination and development of effective methods of transition control can make the transportation vehicles more cost-efficient; moreover, it will be possible to create supersonic passenger airplanes and advanced hypersonic flying vehicles of the new generation.

The initial stage of the transition to turbulence in supersonic boundary layers, which includes the growth of small perturbations and is described by the linear theory of hydrodynamic stability, has been well studied [1, 2], in contrast to nonlinear evolution and interaction of disturbances directly leading to the transition. The capabilities of analytical approaches to studying these phenomena are rather limited, and the experiments in supersonic wind tunnels are rather labor-consuming and expensive. Under these conditions, numerical simulations starts to play a key role. Permanent enhancement of computer power and improvement of numerical algorithms provided a possibility of direct numerical simulation of the transition to turbulence on the basis of solving full three-dimensional Navier–Stokes equations. The first calculations of nonlinear development of perturbations in supersonic boundary layers were performed in the early 1990s [3, 4]. At the moment, numerical simulations can be used to study the processes that occur at all stages of the transition to turbulence: from the stage of transformation of the boundary layer

Khristianovich Institute of Theoretical and Applied Mechanics, Siberian Branch, Russian Academy of Sciences, Novosibirsk, 630090 Russia; khotyanovsky@itam.nsc.ru, alex@itam.nsc.ru. Translated from Prikladnaya Mekhanika i Tekhnicheskaya Fizika, Vol. 58, No. 5, pp. 80–92, September–October, 2017. Original article submitted May 31, 2017.

flow to instability waves of the near-wall shear flow under the action of external acoustic disturbances to the stage of laminar flow breakup due to rapid growth of small-scale three-dimensional oscillations accompanied by flow stochastization, which testifies to the transition to turbulence.

The present paper describes the results of numerical simulations of the transition to turbulence in a supersonic boundary layer at Mach numbers M = 2 and 6, in particular, the transition induced by surface roughness.

FORMULATION OF THE PROBLEM AND NUMERICAL METHOD

The evolution of an unstable supersonic boundary layer on a flat plate is modeled in a computational domain shaped as a rectangular parallelepiped. Three-dimensional unsteady Navier–Stokes equations for a gas with the ratio of specific heats $\gamma = 1.4$ and Prandtl number $\mathrm{Pr} = 0.72$ are solved. The dynamic viscosity μ as a function of temperature T has the form of a power-law dependence with an exponent of 0.76, and the Stokes hypothesis is assumed to be valid for viscous stresses.

The left boundary of the computational domain is located at a certain distance x_0 from the leading edge of the plate, such that the boundary layer in the input section is unstable. Thus, in contrast to other investigations where, in particular, receptivity to external disturbances was considered, here we neglect the effects induced by the presence of a weak shock wave emanating from the leading edge of the plate and its interaction with instability waves.

Two-dimensional simulations of the main flow are first performed; the conditions imposed on the input boundary are the streamwise and transverse velocity and temperature profiles obtained from the self-similar solution of the boundary layer equations. After that the development of unstable disturbances and the transition to turbulence are computed. Instability waves can be excited by different ways, in particular, by means of unsteady injection/suction on a certain region of the plate surface and by using an external source of acoustic waves. In the present study, the flow is excited by unsteady perturbations prescribed at the input boundary as a superposition of eigenfunctions of the linear stability problem, which corresponds to the transition in the case of moderate-amplitude external perturbations, where exponential growth of eigenmodes described by the linear theory prevails at the initial stage of instability development.

In modeling the evolution of three-dimensional disturbances, the side boundaries of the computational domain are subjected to periodic boundary conditions. The spanwise size of the computational domain L_z is taken to be $2\pi/\beta$ (β is the wave number of the disturbance in the z direction). Soft non-reflecting conditions are imposed on the upper ($y = L_y$) and output ($x = x_0 + L_x$) boundaries. To prevent reflection of disturbances from the output boundary, a buffer domain is additionally introduced ahead of this boundary, where artificial relaminarization of the flow is performed by a special technique proposed in [4]. The results of test computations testify to a minor effect of the output boundary on the flow field inside the computational domain. All computations are performed for the plate surface temperature equal to the adiabatic temperature.

The Navier–Stokes equations are solved by using the CFS3D software system developed at the Khristianovich Institute of Theoretical and Applied Mechanics of the Siberian Branch of the Russian Academy of Sciences. The equations are solved on a structured computational grid, which is refined toward the plate surface. The convective fluxes are computed by a fifth-order weighted essentially non-oscillatory (WENO) scheme [5]. The diffusion terms are approximated with the fourth order of accuracy on a compact stencil. Integration with respect to time is performed by the explicit fourth-order Runge–Kutta–Gill scheme [6]. The time step is chosen automatically based on the condition of stability. A detailed description of the method used to solve the Navier–Stokes equations can be found in [7]. The computational algorithm is parallelized by means of geometric decomposition of the computational domain, and the message passing interface (MPI) library is used for data exchange between the processors. Up to 96 cores of a multiprocessor computational cluster were used for the present simulations.

TRANSITION AT THE MACH NUMBER M = 2

It follows from the linear stability theory [1, 2] that only one (the so-called first) mode of disturbances in the boundary layer is unstable at moderate supersonic velocities. Disturbances of this mode are vortex perturba-

tions similar to the Tollmien–Schlichting waves in an incompressible boundary layer. However, in contrast to the incompressible fluid, the most unstable perturbations at M = 2 are three-dimensional disturbances propagating at a sufficiently large angle (50–70°) to the flow.

The mechanisms of instability development in boundary layers at moderate supersonic Mach numbers at subsequent (nonlinear) stages were experimentally investigated in [8–11]. Based on these results, two possible transition scenarios were proposed. The first one is based on resonant interaction of an oblique fundamental wave with a frequency ω_m corresponding to the maximum growth rate coefficient and two subharmonic waves with a frequency $\omega_m/2$, which also propagate at an angle to the flow. Using the relation $\omega = \omega(\alpha, \beta)$ known from the linear theory, one can calculate the angles of propagation of these subharmonics from the phase synchronism conditions. This asymmetric subharmonic resonance was discovered experimentally [10].

The second scenario of the transition was proposed in [12] on the basis of results of direct numerical simulations of disturbance evolution in subsonic and supersonic (M = 1.6) boundary layers. It implies nonlinear interaction of two fundamental waves propagating at angles $\pm\chi$ to the flow. Together with the steady vortex disturbance, these waves form a resonant wave triad. A typical feature of this mechanism is a lower threshold amplitude at which nonlinear interaction of waves begins, resulting in a faster transition. Comparisons of numerical and experimental data [13] confirm the resonance of oblique waves with a steady wave disturbance. Thus, the results reported in [10, 13] testify to the existence of a transition mechanism with a resonance character.

The numerical simulations [12–18] were mainly performed in accordance with the second scenario. The point is that periodic boundary conditions in the spanwise direction cannot be used in subharmonic resonance modeling because the wave number of the fundamental harmonic and subharmonics in this direction are incomparable, generally speaking. As a result, the size of the computational domain along the z axis and, hence, the required computational resources become too large.

In the present calculations, the Reynolds number based on the boundary layer thickness $\delta_0 = \sqrt{\nu_\infty x_0/U_\infty}$ on the input boundary $x = x_0$ was chosen to be $\mathrm{Re} = U_\infty\delta_0/\nu_\infty = 500$, whereas the Reynolds number based on the distance from the leading edge of the plate was $\mathrm{Re}_x = U_\infty x/\nu_\infty = \mathrm{Re}^2 = 2.5 \cdot 10^5$. At these flow parameters, the plate temperature is equal to the adiabatic temperature $T_w/T_\infty = 1.676$ (the subscripts "∞" and w refer to the parameters outside the boundary layer and on the wall, respectively). The streamwise size of the computational domain is $L_x = 3000\delta_0$ and the normal size is $L_y = 100\delta_0$. The computational grid consists of $N_x \times N_y \times N_z = 1024 \times 150 \times 64 \approx 9.8 \cdot 10^6$ cells.

The linear stability characteristics are analyzed for a self-similar basic flow at the input boundary of the computational domain under the assumption of spatial development of disturbances: the disturbances are proportional to $\exp[i(\alpha x + \beta z - \omega t)]$ (ω is the real circular frequency of the disturbance, $\alpha = \alpha_r + i\alpha_i$, α_r and β are the wave vector components along the x and z axes, respectively, $-\alpha_i$ is the growth rate of disturbances, and $\chi = \arctan(\beta/\alpha_r)$ is the angle of disturbance propagation). The frequency parameter $F = \nu_\infty\omega/U_\infty^2$ and the angle χ are varied, which allows one to determine the ranges of parameters of unstable disturbances and parameters of disturbances with the maximum growth rates. The calculated characteristics of linear stability for this case were reported in [18].

A superposition of two unstable disturbances propagating at the angles $\chi = \pm 55°$ to the basic flow was imposed onto the latter. The dimensionless frequency of disturbances $F = 6.2 \cdot 10^{-5}$ is the frequency at which the growth rate reaches its maximum value, and the amplitude is 0.5% of the free-stream velocity. The simulated evolution of such a disturbed flow is illustrated in Fig. 1.

The development of disturbances includes several stages. When the linear stage is finalized, a secondary flow is formed from streamwise vortex structures whose characteristic sizes in the normal and transverse directions are of the order of the boundary layer thickness. It should be noted that the formation of such structures was also observed in [4]. It follows from the analysis of cross-sectional vorticity distributions that the streamwise vortices first evolve independent of each other, but their transverse sizes slowly increase as they move downstream. At a certain time, the entire transverse flow field becomes involved into vortex motion.

After that the secondary instability starts to develop, which includes rapid growth of three-dimensional fluctuations leading to the laminar–turbulent transition. The instantaneous fields of gas-dynamic variables acquire a random character (see Fig. 1).

The mean velocity profiles obtained after averaging with respect to time (over an interval equal to eight periods of the imposed disturbance) and with respect to L_z are shown in Fig. 2. It is seen that the velocity profile

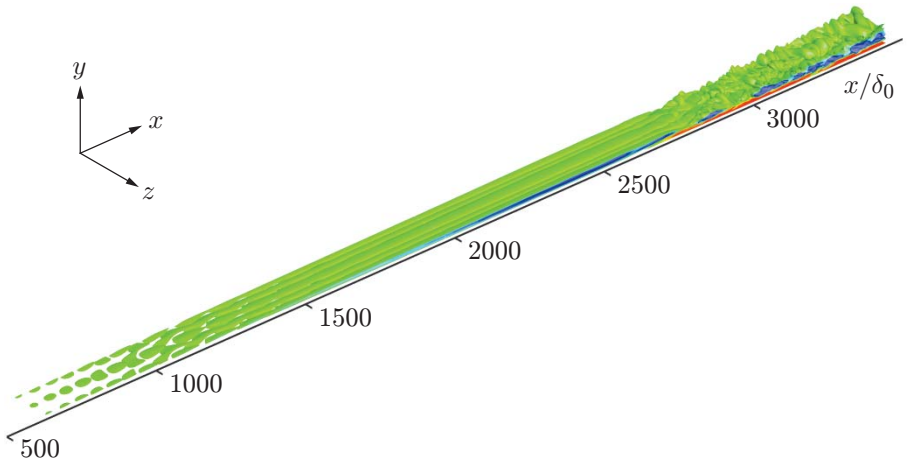

Fig. 1. Isosurfaces of oscillations of the streamwise velocity component in the case of nonlinear development of the disturbance in the form of a superposition of three-dimensional instability waves (M = 2).

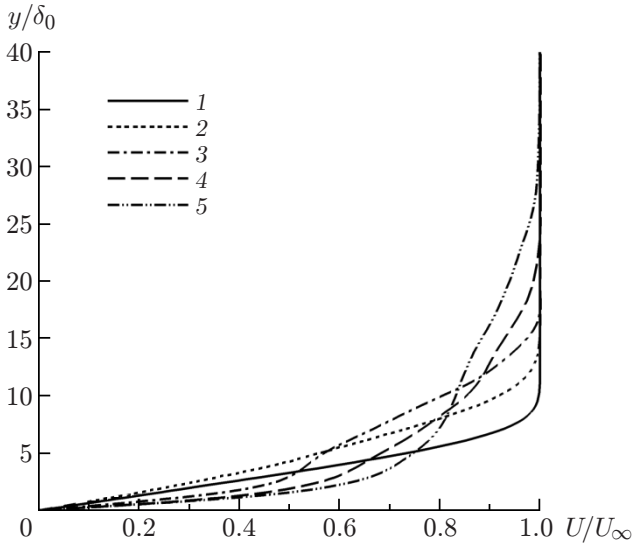

Fig. 2.

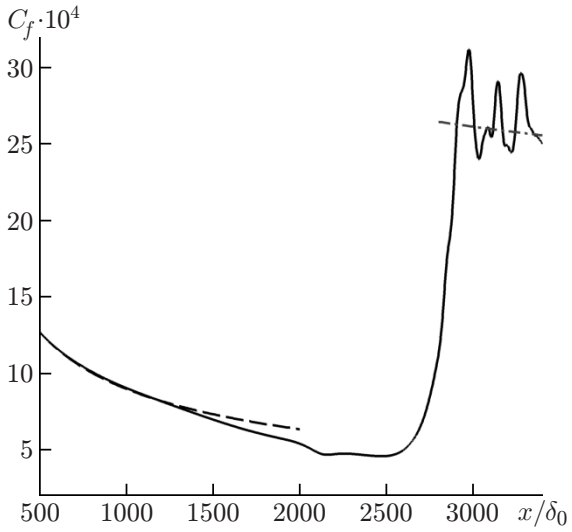

Fig. 3.

Fig. 2. Mean velocity profiles in different cross sections (M = 2): x/δ_0 = 1000 (*1*), 2000 (*2*), 2800 (*3*), 3000 (*4*), and 3400 (*5*).

Fig. 3. Distribution of the friction coefficient along the plate (M = 2): the solid curve shows the results of direct numerical simulation; the dashed and dot-and-dashed curves show the results calculated for the laminar and turbulent boundary layers, respectively.

corresponding to the laminar boundary layer, which almost coincides with the profile corresponding to the self-similar solution of the boundary layer equations, transforms to an intermediate profile including an inflection point and then becomes more filled, which is closer to the profile corresponding to the turbulent boundary layer.

Figure 3 shows the distribution of the mean skin friction coefficient C_f along the plate and the corresponding distributions for the self-similar, laminar, and developed turbulent boundary layers (the last calculation was performed by a semi-empirical method proposed in [19]). It is seen that the friction coefficient at $x/\delta_0 \lesssim 1500$ agrees

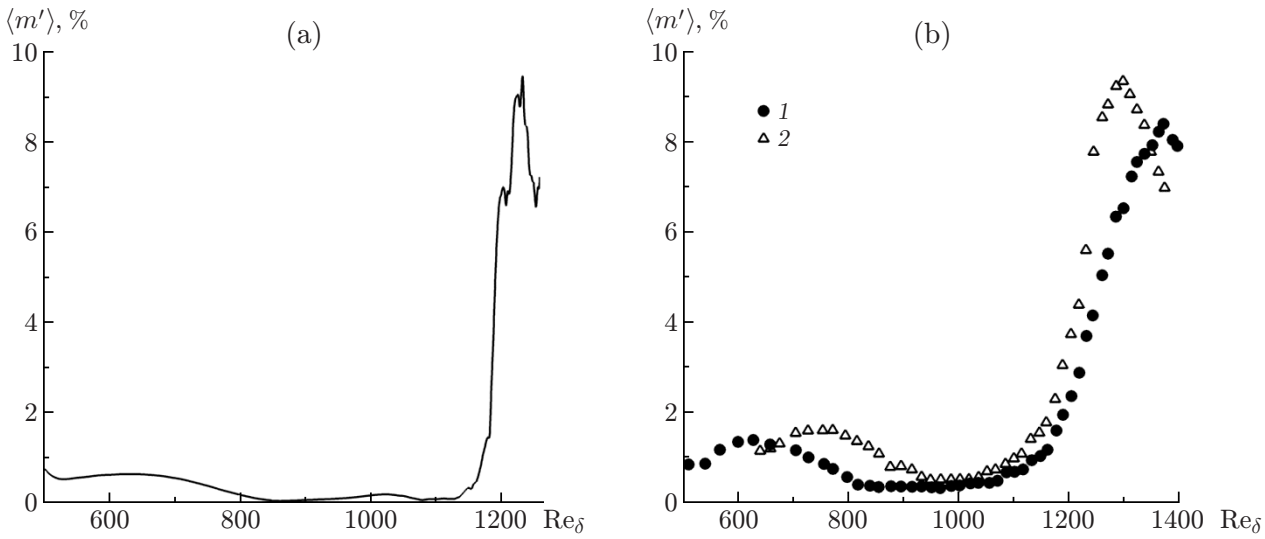

Fig. 4. Root-mean-square fluctuations of the mass flow rate $\langle m' \rangle$ versus the Reynolds number based on the local thickness of the boundary layer Re_δ in the calculation (a) and experiments in the presence of disturbances at the unit Reynolds number $\mathrm{Re}_1 = 6.8 \cdot 10^6$ m^{-1} [11] (b): natural (*1*) and artificial (*2*) disturbances.

well with the value of C_f corresponding to the laminar case. At $x/\delta_0 \approx 2700$, the friction coefficient drastically increases (by a factor of 5–6), which corresponds to the instant of the laminar–turbulent transition. After the transition, the value of C_f fluctuates and decreases, approaching the value corresponding to a developed turbulent flow. The transition also leads to a significant increase in the momentum thickness (more than twice as compared to the value for the laminar flow).

Figure 4 shows the distributions of the root-mean-square fluctuations of the mass flow rate, which were calculated in the present work and obtained experimentally in [11]. It is evident that direct numerical simulation accurately reproduces the distribution of fluctuations over the streamwise coordinate. In particular, it should be noted that there is a local peak of the intensity of mass flow rate fluctuations both in the calculation (at $\mathrm{Re} \approx 650$) and in the experiments (at $\mathrm{Re} \approx 630$ in the case of natural disturbances and at $\mathrm{Re} \approx 760$ in the case of artificial disturbances). The Reynolds numbers at the point of the laminar–turbulent transition in the calculation and experiments are very close to each other: $\mathrm{Re}_{tr} \approx 1150$. It can be expected that the transition point location substantially depends on the initial amplitude of the disturbance, which determines the length of the linear growth region. However, the positions of this point in the experiments [11] are close to each other, regardless of whether the flow is excited by natural or localized artificial perturbations. The location of the transition point in the calculation in the case of flow excitation by spanwise-periodic disturbances corresponding to the eigenfunctions of the linear stability theory turned out to be approximately the same. This method of flow excitation corresponds to the second scenario of the transition.

TRANSITION AT THE MACH NUMBER M = 6

The pattern of boundary layer stability at hypersonic Mach numbers is substantially different from the pattern observed at moderate supersonic velocities. In accordance with the linear stability theory and experimental data, the key role in the laminar–turbulent transition at high Mach numbers belongs to second-mode disturbances, which were first identified in [1, 2]. Two-dimensional disturbances of the second mode have the greatest growth rates. Oblique three-dimensional disturbances of the first and second modes are also unstable, but their growth rates are much smaller. Second-mode disturbances of a given frequency remain unstable in a rather narrow range of Reynolds numbers. They are expected to stabilize rapidly as they move downstream. Vice versa, three-dimensional disturbances of the first mode, which have smaller growth rates, can remain unstable at large distances. Thus, the linear dynamics of instability of a hypersonic boundary layer describes the mechanism of the competition of

different disturbance modes. Nonlinear interaction of instability waves at the next stages makes the wave pattern even more complicated; as a result, various transition scenarios are possible, depending on the upstream conditions.

Numerical and experimental investigations of the evolution of unstable disturbances in boundary layers at high Mach numbers were performed in [20–32]. Various aspects were studied: development of unstable acoustic disturbances of the second mode [20–22], receptivity of the boundary layer transition to external acoustic perturbations [23–25], influence of localized heating and cooling of the wall on the second-mode disturbances [26], effect of surface porosity on flow stability and laminar–turbulent transition, and suppression of unstable acoustic disturbances by using porous coatings [27–29]. As the greatest growth rates at high Mach numbers are observed for two-dimensional disturbances, the numerical study of the initial stages of the laminar–turbulent transition can be performed in a two-dimensional formulation [30, 31]. It is clear, however, that the transition occurs in the case of significant three-dimensional oscillations of the flow field. As the development of two-dimensional disturbances of the second mode does not include a mechanism of generation of three-dimensional oscillations, it may be assumed that the onset of turbulence is a consequence of simultaneous development of disturbances of different modes. At the initial part of the plate, two-dimensional second-mode disturbances are rapidly enhanced, and disturbances of lower frequencies are gradually involved into the process as the boundary layer thickness increases. The amplitudes of the oblique waves of the first-mode disturbances grow significantly slower, but these waves generate three-dimensional fluctuations necessary for transition initiation.

In the present computation, the input boundary of the computational domain was placed in the cross section where $\mathrm{Re} = U_\infty \delta_0/\nu_\infty = 1000$. The wall temperature $T_w/T_e = 7.053$ was equal to the temperature of an adiabatically isolated plate in a laminar flow. The computational domain had the sizes $L_x = 4500\delta_0$ and $L_y = 150\delta_0$; the size L_z was equal to the disturbance wavelength along the z axis. The number of cells of the computational grid was $N_x \times N_y \times N_z = 2304 \times 250 \times 72 \approx 41.4 \cdot 10^6$.

It follows from the linear stability calculations performed for this case in [32] that the neutral curves have two segments at $\chi = 0^\circ$: a segment of high-frequency disturbances corresponding to the second-mode acoustic disturbances and a segment of low-frequency disturbances corresponding to the first-mode vortex disturbances. The growth rates of the first-mode disturbances are smaller by an order of magnitude. As the angle χ increases, the growth rates of the second-mode disturbances decrease, while those of the first-mode disturbances increase, but their maximum value reached at $\chi = 62^\circ$ is approximately three times smaller than the growth rates of the two-dimensional disturbances of the second mode.

In direct numerical simulations, the flow was excited by a superposition of a two-dimensional disturbance of the second mode with the frequency $F = 10^{-4}$ and two symmetric first-mode waves with the frequency $F = 0.5 \cdot 10^{-4}$ propagating at the angles $\chi = \pm 57^\circ$ to the flow. It follows from the results calculated for $\chi = 57^\circ$ that the growth rate of the first mode is close to the maximum value, whereas the second-mode disturbances are stable [32]. The initial amplitudes of disturbances are approximately 0.5% of the free-stream velocity. The two-dimensional disturbance frequency was chosen to be small as compared to the frequency of the wave with the maximum growth rate so that the disturbance remained unstable at a sufficiently large distance from the input cross section.

The calculation shows that the two-dimensional second-mode disturbances dominate at the initial stage and rapidly grow. The effect of the first-mode disturbances, which grow appreciably slower, is mainly manifested as periodic deformation of initially flat "rollers" of the second-mode disturbances in the transverse direction. Figure 5 shows the vorticity regions visualized as an isosurface of the Q-criterion (half-difference of the squared norms of the vorticity tensor and strain rate tensor) [33]. When the growth of the second-mode disturbances ceases because of the increase in the boundary layer thickness, the first-mode disturbances continue to grow. Thus, the three-dimensional component of the secondary flow formed due to a multiple increase in the amplitude of the oscillations of the second mode and its subsequent stabilization continues to increase.

As three-dimensional fluctuations are enhanced, horseshoe vortex structures protruding from the boundary layer are formed, which is consistent with the results of modeling the transition to turbulence at the Mach number $\mathrm{M} = 4.5$ in [4]. Further downstream ($x/\delta_0 \approx 3000$), the growth of the three-dimensional disturbances leads to breakdown of the unstable boundary layer and to the laminar–turbulent transition, which is manifested as rapid growth of small-scale fluctuations and significant changes in all characteristics of the boundary layer. Figure 6 shows the profiles of the mean streamwise velocity in several cross sections corresponding to the laminar ($x/\delta_0 \leqslant 3000$), transitional, and turbulent ($x/\delta_0 \geqslant 4000$) flows.

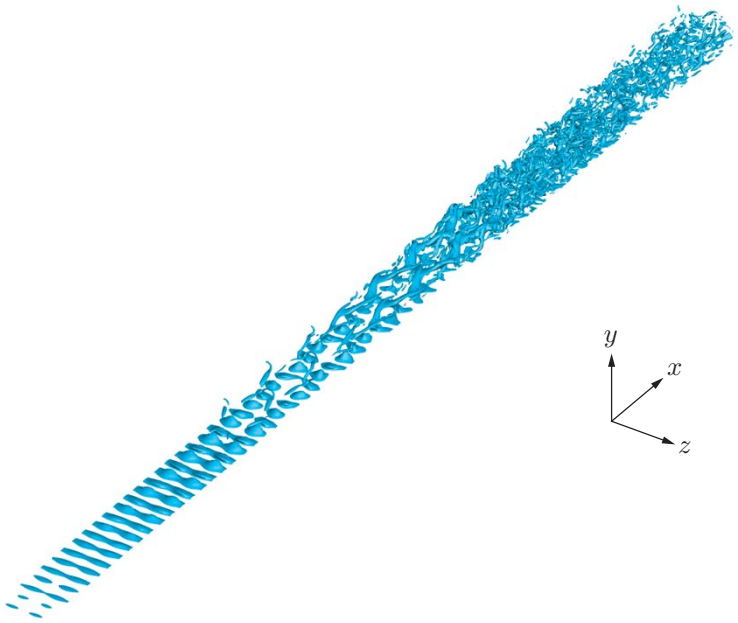

Fig. 5. Isosurfaces corresponding to the Q-criterion in the case of nonlinear development of a disturbance in the form of a superposition of a two-dimensional wave of the second mode and three-dimensional waves of the first mode (M = 6).

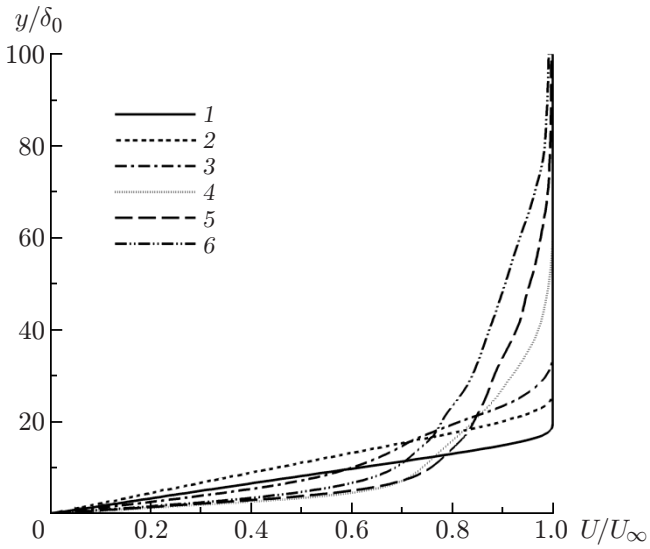

Fig. 6.

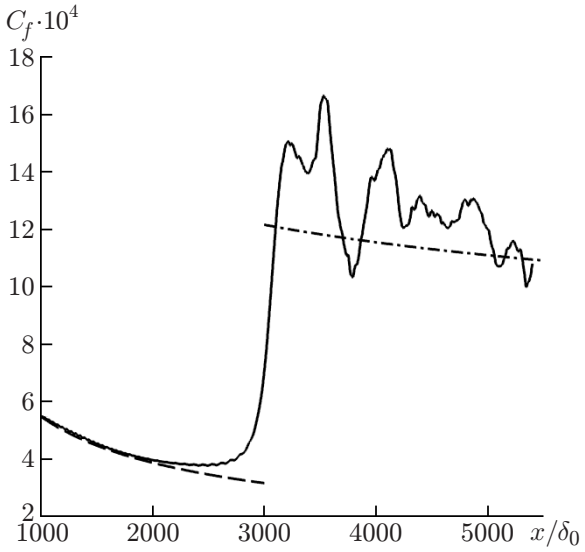

Fig. 7.

Fig. 6. Mean velocity profiles in different cross sections (M = 6): x/δ_0 = 1100 (*1*), 2000 (*2*), 3000 (*3*), 4000 (*4*), 5000 (*5*), and 5400 (*6*).

Fig. 7. Distributions of the friction coefficient along the plate (M = 6): the solid curve shows the results of direct numerical simulation; the dashed and dot-and-dashed curves show the results calculated for the laminar and turbulent boundary layers, respectively.

During the transition to the turbulent flow regime, the skin friction coefficient increases almost by a factor of 4 (Fig. 7). After the transition, the value of C_f fluctuates and approaches the value corresponding to the turbulent flow.

ROUGHNESS-INDUCED TRANSITION

It is known that one of the most important factors affecting the transition to turbulence in the boundary layer is the surface roughness. In supersonic and hypersonic flight modes, the presence of roughness caused by structural features of the aircraft surface, ablation, contamination, and other reasons may speed up the transition to turbulence and lead to a significant increase in the drag force and heat fluxes [34]. The influence of roughness is most pronounced near the aircraft tip and leading edges, where the size of the roughness elements is comparable with the boundary layer thickness.

The experimental [35] and numerical [36, 37] investigations of flow instability behind an individual roughness element showed that streamwise structures are formed in the boundary layer due to mean flow excitation because of the presence of such an element. These structures exist for a long time, which leads to the development of new types of instability.

In this work, we study the influence of distributed roughness on the laminar–turbulent transition in the boundary layer at the Mach number M = 2. The problem formulation is basically similar to that used for modeling the transition on a smooth flat plate. These two situations differ by the fact that no perturbations are introduced into the basic flow at the input boundary of the computational domain (corresponding to the Reynolds number based on the boundary layer thickness $\mathrm{Re} = U_\infty \delta_0/\nu_\infty = 500$). Instead, a band of width $100\delta_0$ with randomly distributed roughness elements is placed across the computational domain at a certain distance from the input boundary. The shape of the roughness elements is defined by the function $y = h\cos^2(\pi r/(2R))$, where r is the distance from the roughness element center in the plane (x, z). The radius $\delta_0 \leqslant R \leqslant 10\delta_0$ and the height $\delta_0 \leqslant h \leqslant R$ of the roughness element are random variables, which take various values within the above-indicated ranges. The roughness distribution on the plate surface is shown in Fig. 8. The influence of the roughness elements on the generation of

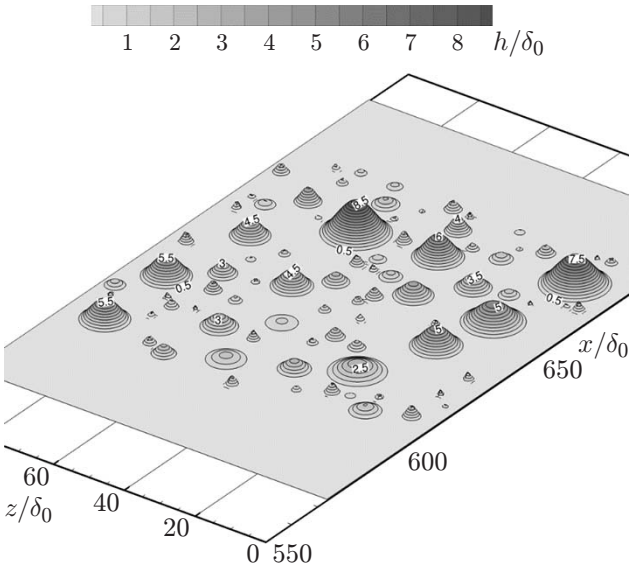

Fig. 8.

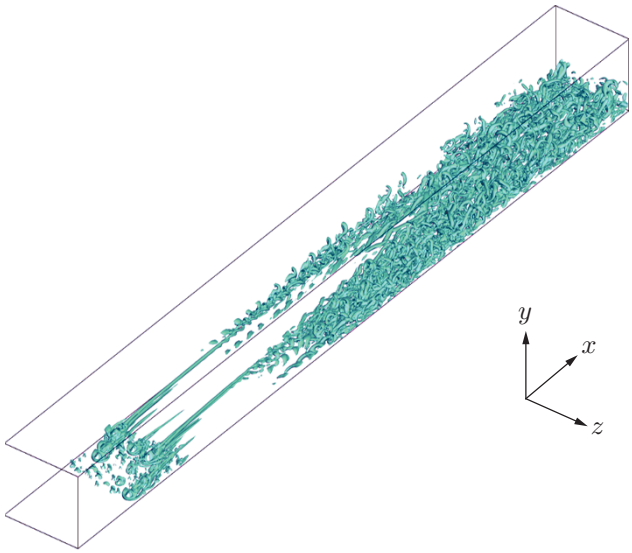

Fig. 9.

Fig. 8. Random distribution of roughness on the plate surface.

Fig. 9. Isosurfaces corresponding to the Q-criterion during the transition to turbulence in a supersonic (M = 2) boundary layer initiated by surface roughness.

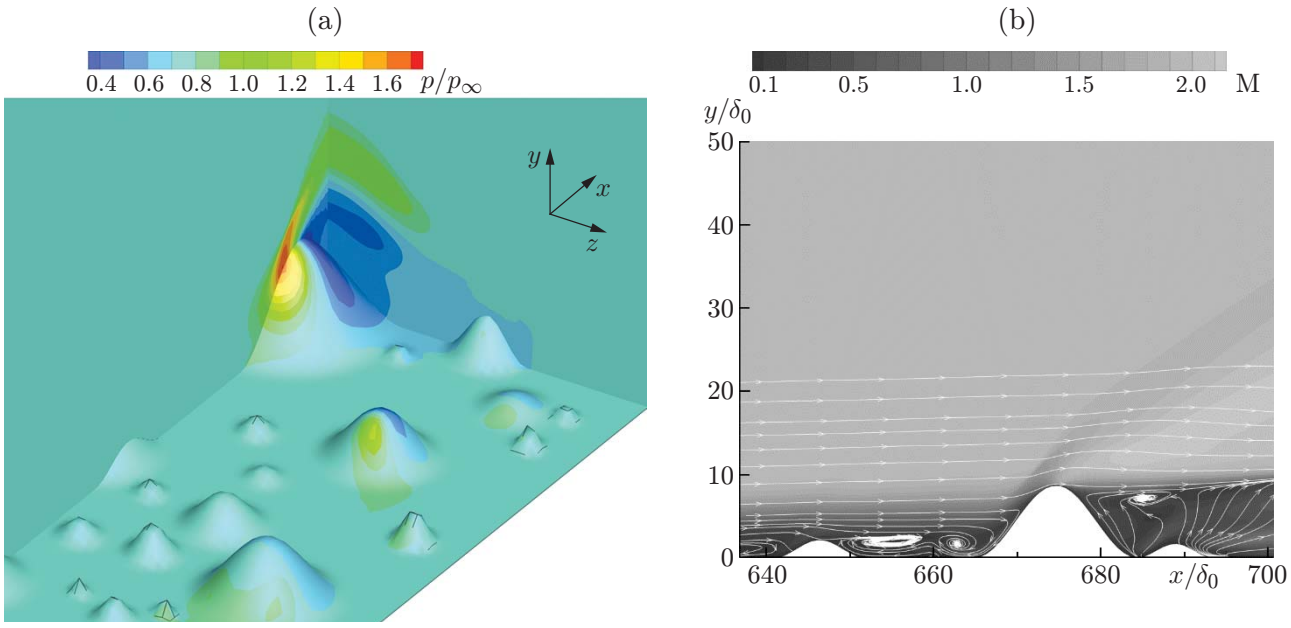

Fig. 10. Flow near a large roughness element: (a) pressure field; (b) local Mach number field and streamlines.

disturbances in the boundary layer is usually characterized by the dimensionless parameter $\mathrm{Re}_{kk} = U_h h/\nu_h$, which is the Reynolds number based on the roughness element height and on the values of velocity and viscosity in the laminar boundary layer at this height [34–37]. At the above-given roughness levels, the value of Re_{kk} varies in the interval from 40 to 5000. In the case considered here, the sonic line in the laminar boundary layer is located at the height $y = 2.85\delta$; therefore, some roughness elements are submerged into the subsonic region of the boundary layer, whereas some other roughness elements protrude into the supersonic region.

The computation was performed in a computational domain with $L_x = 1000\delta_0$, $L_y = 75\delta_0$, and $L_z = 100\delta_0$ on a surface-fitted grid consisting of $N_x \times N_y \times N_z = 1280 \times 200 \times 128 \approx 32.7 \cdot 10^6$ cells. The resultant instantaneous flow field is shown in Fig. 9. Local perturbations of the flow field near the roughness elements are manifested as steady horseshoe structures, and the formation of streamwise vortex structures is observed in the wake behind the roughness elements. The intensity of the formed vortices depends on the roughness element size. The most pronounced effect on generation of vortex disturbances is exerted by elements with heights $h > 3\delta_0$, which corresponds to $\mathrm{Re}_{kk} > 500$.

Figure 10 shows the flow field near a large roughness element with the height $h \approx 8\delta_0$ and the vortex wake, which develops behind it. The upper part of the element protrudes to the supersonic region of the boundary layer. As a result, a weak shock arises ahead of the windward side of the roughness element and an expansion fan is formed on the leeward side. The shock intensity during its propagation in the external flow rapidly decreases due to its interaction with the expansion fan.

A high-pressure spot appears directly behind the shock wave on the windward side of the roughness element. An increase in pressure makes the gas spread down the slope and in the side directions. The downward flow of the gas leads to the formation of a recirculation region near the foot of the element. A secondary recirculation region behind the element is formed owing to interaction with the flow around a smaller roughness element located upstream. These recirculation regions serve as sources of unsteady disturbances.

The vortex structures in the wake behind large roughness elements transform further downstream to intense streamwise vortices giving rise to large gradients of flow parameters. The resultant secondary flow includes free shear layers prone to the action of inviscid instability. Unsteady oscillations arising in the recirculation regions can serve as a source of instability in regions of vortex motion. It is seen in Fig. 9 that three-dimensional disturbances slowly grow in the streamwise vortices at a certain distance downstream from the roughness band. When the amplitudes of these disturbances reach sufficiently large values, vortex breakdown occurs (the vortices start to interact with each other by that time). All these factors lead to explosive growth of small-scale three-dimensional oscillations and to the laminar–turbulent transition.

CONCLUSIONS

Direct numerical simulations of the laminar–turbulent transition in supersonic and hypersonic (M = 2 and 6) boundary layers were performed, including the early linear stages, later nonlinear stages, laminar flow failure, stochastization, and transition to turbulence.

The transition scenario at M = 2 includes the formation of elongated vortex structures due to nonlinear evolution of two symmetric instability waves, resulting at a certain distance in rapid growth of small-scale three-dimensional oscillations and finally in the transition to turbulence. The predicted transition point location agrees well with the position of this point detected experimentally.

At M = 6, two-dimensional disturbances of the second mode dominate at the early stages of the transition and rapidly grow. The influence of three-dimensional disturbances is manifested as a modulation of the disturbed field of the prevailing second mode and generation of three-dimensional fluctuations. Instability development proceeds faster if the boundary layer is excited by a superposition of disturbances of the first and second modes. Three-dimensional disturbances continue to grow downstream until the transition occurs. The laminar–turbulent transition at M = 6 is observed at a considerably greater distance from the leading edge than at M = 2.

Direct numerical simulations of the flow past a rough surface in a supersonic boundary layer at M = 2 were also performed. The presence of roughness leads to excitation of the mean flow and to the onset of unsteady processes in the wake behind the roughness element. Owing to induced gradients of velocity, streamwise vortex structures are formed in the wake. The downstream evolution of the vortex structures is accompanied by the development of instability of shear layers, resulting in the emergence of unsteady three-dimensional oscillations. The most significant disturbances are induced by roughness elements with heights $h > 3\delta$, which corresponds to $\mathrm{Re}_{kk} > 500$. Further downstream, the evolution of disturbances in streamwise vortex structures and interaction of the neighboring vortices lead to the laminar–turbulent transition.

This work was supported by the Russian Science Foundation (Grant No. 14-11-00490 p). The computations were performed at the computational cluster of the Novosibirsk State University.

REFERENCES

1. L. M. Mack, "Boundary-Layer Stability Theory: JPL Report," Jet Propulsion Lab.; No. 90-277-REV-A (NASA, Pasadena, 1969), CR 131501.
2. S. A. Gaponov and A. A. Maslov, *Development of Disturbances in Compressible Flows* (Nauka, Novosibirsk, 1980) [in Russian].
3. G. Erlebacher and M. G. Hussaini, "Numerical Experiments in Supersonic Boundary-Layer Stability," Phys. Fluids A **1** (1), 94–104 (1990).
4. N. A. Adams, "Direct Numerical Simulation of Turbulent Compression Ramp Flow," Theoret. Comput. Fluid Dynamics **12**, 109–129 (1998).
5. G. S. Jiang and C.-W. Shu, "Efficient Implementation of Weighted ENO Schemes," J. Comput. Phys. **26**, 202–228 (1996).
6. E. Hairer, S. P. Norsett, and G. Wanner, *Solving Ordinary Differential Equations: Nonstiff Problems* (Springer Verlag, 1987).
7. A. N. Kudryavtsev, T.V. Poplavskaya, and S. V. Khotyanovsky, "Application of High-Order Schemes for Simulating Unsteady Supersonic Flows," Mat. Model. **19** (7), 39–55 (2007).
8. J. Laufer and T. Vrebalovich, "Stability and Transition of a Supersonic Laminar Boundary Layer on an Insulated Plate," J. Fluid Mech. **9**, 257–299 (1960).
9. A. D. Kosinov, A. A. Maslov, and S. G. Shevelkov, "Experiments on the Stability of Supersonic Laminar Boundary Layers," J. Fluid Mech. **219**, 621–633 (1990).
10. A. D. Kosinov, N. V. Semionov, S. G. Shevelkov, and O. I. Zinin, "Experiments on Instability of Supersonic Boundary Layers," in *Nonlinear Instability of Nonparallel Flows* (Springer, Berlin–Heidelberg, 1994), pp. 196–205.
11. Yu. G. Ermolaev, A. D. Kosinov, and N. V. Semionov, "Typical Features of Weakly Nonlinear Interaction of Instability Waves in a Supersonic Boundary Layer," Vestn. Novosib. Univ. Ser. Fizika **3** (3), 3–13 (2008).
12. A. Thumm, W. Wolz, and H. Fasel, "Numerical Simulation of Spatially Growing Three-Dimensional Disturbance Waves Incompressible Boundary Layers," in *Laminar-Turbulent Transition* (Springer, Berlin–Heidelberg, 1993), pp. 303–308.

13. C. S. J. Mayer, S. Wernz, and H. F. Fasel, "Investigation of Oblique Breakdown in a Supersonic Boundary Layer Using DNS," AIAA Paper No. 2007-0949 (Reno, 2007).
14. N. D. Sandham and N. A. Adams, "Numerical Simulation of Boundary-Layer Transition at Mach Two," Appl. Sci. Res. **51**, 371–375 (1993).
15. N. D. Sandham, N. A. Adams, and L. Kleiser, "Direct Simulation of Breakdown to Turbulence Following Oblique Instability Waves in a Supersonic Boundary Layer," Appl. Sci. Res. **54**, 223–234 (1995).
16. C. S. J. Mayer, S. Wernz, and H. F. Fasel, "Numerical Investigation of the Nonlinear Transition Regime in a Mach 2 Boundary Layer," J. Fluid Mech. **668**, 113–149 (2011).
17. C. S. J. Mayer, D. A. von Terzi, and H. F. Fasel, "Direct Numerical Simulation of Investigation of Complete Transition to Turbulence via Oblique Breakdown at Mach 3," J. Fluid Mech. **674**, 5–42 (2011).
18. A. N. Kudryavtsev and D. V. Khotyanovsky, "Direct Numerical Simulation of Transition to Turbulence in a Supersonic Boundary Layer," Teplofiz. Aeromekh. **22** (5), 581–590 (2015) [Thermophys. Aeromech. **22** (5), 559–568 (2015)].
19. Yu. V. Lapin, *Turbulent Boundary Layer in Supersonic Gas Flows* (Nauka, Moscow, 1982) [in Russian].
20. C. D. Pruett, T. A. Zang, C.-L. Chang, and M. H. Carpenter, "Spatial Direct Numerical Simulation of High-Speed Boundary-Layer Flows. Pt 1. Algorithmic Considerations and Validation," Theoret. Comput. Fluid Dynamics **7**, 49–76 (1995).
21. N. A. Adams and L. Kleiser, "Subharmonic Transition to Turbulence in a Flat-Plate Boundary Layer at Mach Number 4.5," J. Fluid Mech. **317**, 301–335 (1996).
22. A. Maslov, D. Bountin, A. Shiplyuk, et al., "Experimental Study of Compressible Boundary Layer on a Cone at Angles of Attack," Acta Mech. Sinica. **25** (3), 325–333 (2009).
23. A. A. Maslov, A. N. Shiplyuk, A. A. Sidorenko, and D. Arnal, "Leading-Edge Receptivity of a Hypersonic Boundary Layer on a Flat Plate," J. Fluid Mech. **426**, 73–94 (2001).
24. Y. Ma and X. Zhong, "Receptivity of a Supersonic Boundary Layer over a Flat Plate. Pt 1. Wave Structures and Interactions," J. Fluid Mech. **488**, 31–78 (2003).
25. Y. Ma and X. Zhong, "Receptivity of a Supersonic Boundary Layer over a Flat Plate. Pt 2. Receptivity to Free-Stream Sound," J. Fluid Mech. **488**, 79–121 (2003).
26. A. Fedorov, V. Soudakov, I. Egorov, et al., "High-Speed Boundary-Layer Stability on a Cone with Localized Wall Heating or Cooling," AIAA J. **53** (9), 2512–2524 (2015).
27. A. Shiplyuk, A. Maslov, E. Burov, and N. Malmuth, "Stabilization of a Hypersonic Boundary Layer Using an Ultrasonically Absorptive Coating," J. Fluid Mech. **479**, 99–124 (2003).
28. I. V. Egorov, A. V. Fedorov, and V. G. Soudakov, "Receptivity of a Hypersonic Boundary Layer over a Flat Plate with a Porous Coating," J. Fluid Mech. **601**, 165–187 (2008).
29. A. A. Maslov, A. V. Fedorov, D. A. Bountin, et al., "Experimental Study of Disturbances in Transitional and Turbulent Hypersonic Boundary Layers," AIAA J. **46** (7), 1880–1883 (2008).
30. I. V. Egorov, V. G. Soudakov, and A. V. Fedorov, "Numerical Simulation of Propagation of Disturbances in a Supersonic Boundary Layer," Izv. Ross. Akad. Nauk. Mekh. Zhidk. Gaza, No. 6, 33–44 (2004).
31. I. V. Egorov, A. V. Fedorov, and V. G. Soudakov, "Direct Numerical Simulation of Disturbances Generated by Periodic Suction-Blowing in a Hypersonic Boundary Layer," Theoret. Comput. Fluid Dynamics **20**, 41–54 (2006).
32. A. N. Kudryavtsev and D. V. Khotyanovsky, "Numerical Simulation of the Evolution of Various Modes and Initial Stages of the Laminar–Turbulent Transition in the Boundary Layer at the Freestream Mach Number M = 6," Teplofiz. Aeromekh. **23** (6), 843–852 (2016) [Thermophys. Aeromech. **23** (6), 809–818 (2016)].
33. M. Lesieur, O. Metais, and P. Comte, *Large-Eddy Simulations of Turbulence* (Cambridge Univ. Press, Cambridge, 2005).
34. S. P. Schneider, "Effects of Roughness on Hypersonic Boundary-Layer Transition," J. Spacecraft Rockets **45** (2), 193–209 (2008).
35. B. M. Wheaton and S. P. Schneider, "Roughness-Induced Instability in a Hypersonic Laminar Boundary Layer," AIAA J. **50** (6), 1245–1256 (2012).
36. M. Choudhari, A. Norris, F. Li, et al., "Wake Instabilities behind Discrete Roughness Elements in High Speed Boundary Layers," AIAA Paper No. 2013-0081 (Grapevine, 2013).
37. H. B. E. Kurz and M. J. Kloker, "Mechanisms of Flow Tripping by Discrete Roughness Elements in a Swept-Wing Boundary Layer," J. Fluid Mech. **796**, 158–194 (2016).